hybrid and nearby f_q frequencies, with consequent and obvious diagnostic implications. The coexistence of the banded, and $(n+\frac{1}{2})f_{ce}$ signals shows that the classification of magnetospheric instabilities is more complex than the current conjecture[4] that both emissions are basically the same phenomenon, occurring in different regions of the magnetosphere.

We thank M. Petit, B. de la Porte, R. Grard, A. Pedersen, M. Debrie, F. Lefeuvre, M. Hamelin, A. Bahnsen, E. Ungstrupp, G. Wrenn, H. Borg and F. Mariani for their valuable scientific collaboration. The contributions of the European Space Operations Centre, the Centre National d'Etudes Spatiales, Toulouse, E. Gershuny and J. Hunter of Sussex University to the data handling are acknowledged, as is the work of K. Knott, project Scientist, and the Geos project team. This research is supported by the SRC, CNET, CNRS, France, and ESA.

Received 29 March; accepted 30 March 1978.

1. Knott, K. *ESRO Rep. 17th Cospar Mtng*. Sao Paulo, Brazil, 162 (1974).
2. Etcheto, J. & Petit, M. *C.r. hebd. Acid. Sci. Paris*, **285B**, 329 (1977).
3. Bernstein, I. B. *Phys. Rev.* **109**, 10 (1958).
4. Shaw, R. & Gurnett, D. A. *J. geophys. Res.* **80**, 4259 (1975).
5. Kennel, C. F., Scarf, F. L., Fredericks, R. W., McGhee, J. H. & Coronite, F. V. *J. geophys. Res.* **75**, 6136 (1970).
6. Tataronis, J. A. & Crawford, F. W. *J. Plasma Phys.* **4**, 231, 249 (1970).
7. Bekefi, G. *Radiation Process in Plasmas* (Wiley, New York, 1966).
8. Trulsen, J. *J. Plasma Phys.* **6**, 367 (1971).

Image reconstruction from incomplete and noisy data

S. F. Gull & G. J. Daniell*

Mullard Radio Astronomy Observatory, Cavendish Laboratory, Madingley Road, Cambridge, UK

Results are presented of a powerful technique for image reconstruction by a maximum entropy method, which is sufficiently fast to be useful for large and complicated images. Although our examples are taken from the fields of radio and X-ray astronomy, the technique is immediately applicable in spectroscopy, electron microscopy, X-ray crystallography, geophysics and virtually any type of optical image processing. Applied to radioastronomical data, the algorithm reveals details not seen by conventional analysis, but which are known to exist.

In many branches of physics, such as spectroscopy, X-ray crystallography and radioastronomy, the primary data are the Fourier transform of the physical quantities which are of interest. The inverse Fourier transform is normally then calculated with a digital computer. It is perhaps unfortunate that this calculation is so simple and fast, because it encourages the belief that this is the best way to use the data. However, because the data can never in practice be obtained for the whole range of the transform variable, and can never be free from experimental errors, other possibilities need to be explored.

We have used an alternative method of analysis, based on the idea of maximum entropy, which is illustrated using data produced by the radio telescopes at the Mullard Radio Astronomy Observatory. In this application the data are samples of the two-dimensional Fourier transform of the radio brightness from the sky. We then show how the method may be modified to deal with data not involving a Fourier transform, and apply it to an X-ray map of the supernova remnant Cassiopeia A.

Safe inversion techniques

The correct formulation of problems involving incomplete and noisy data lies in the field of inverse theory. Previously, inverse problems have frequently been tackled by fitting empirical models, although this often leads to false confidence in the conclusions obtained. A notable advance is the method of Backus and Gilbert, which is most clearly explained in the general review by Parker[1]. This method shows explicitly the inevitable compromise that must be made between spatial resolution and the accuracy of amplitude measurements, and protects the user against making deductions that are not warranted by the data. This method has been applied to the evaluation of Fourier transforms by Oldenburg[2].

*Permanent address: Department of Physics, The University, Southampton, UK.

To avoid abstraction, we shall refer to our radioastronomical example. Starting with incomplete and noisy data, one can obtain by the Backus–Gilbert method a series of maps of the distribution of radio brightness across the sky, all of which are consistent with the data, but have different resolutions and noise levels. From the data alone, there is no reason to prefer any one of these maps, and the observer may select the most appropriate one to answer any specific question. Hence, the method cannot produce a unique 'best' map of the sky. There is no single map that is equally suitable for discussing both accurate flux measurements and source positions.

Nevertheless, it is useful to have a single general-purpose map of the sky, and the maximum-entropy map described here fulfils this role. Although it cannot be thought of as the true sky convolved with any beamshape, we believe that the maximum-entropy map may be used with confidence to describe the general appearance of the sky and that, like the Backus–Gilbert maps, it cannot lead to conclusions for which there is evidence in the data.

The advantages of the maximum-entropy map are: that the radio intensity is shown as everywhere positive, in spite of noise in the data; that sidelobes are automatically reduced to a very low level; the maximum resolution consistent with the physical size of the telescope is obtainable; that the resulting map is smooth; that regions of low surface brightness are clearly shown and are not confused by noise; the method is applicable to the cases where the phases of the Fourier components are either inaccurate or entirely unknown.

The maximum-entropy solution

The origins of our method are given elsewhere[3–6]. We shall not give quasi-philosophical arguments concerning maximum entropy in this context, but the following discussion shows in physical terms what our mathematics describes. Although we discuss the maximum-entropy method in the radioastronomical context it will be apparent how the method can be applied in other circumstances.

As in statistical mechanics, we introduce quantisation to simplify the counting of states, so we divide the sky into small areas, and quantise the radio intensity. We now imagine the traditional 'team of monkeys' who produce random trial maps by scattering quanta of radio intensity across the cells of the sky. This is done without regard to observations, and produces a large pile containing, many times over, all positive trial maps of the sky. We take their Fourier transforms, and compare these with the data. Almost all of the trial maps will be inconsistent with the data despite the observational errors, and these we reject. Those which are left, and are compatible with the given data and the errors, are

0028–0836/78/0272—0686$01.00

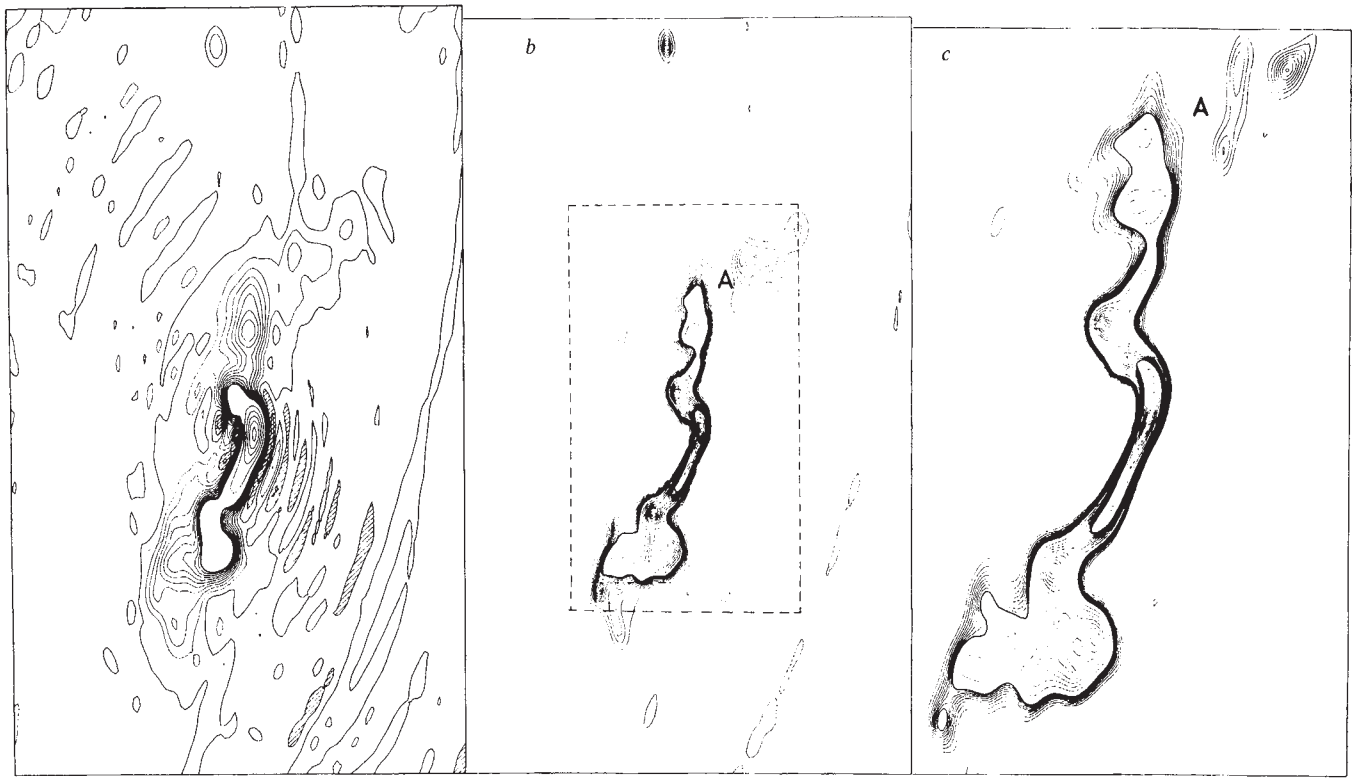

Fig. 1 *a*, Conventional map of the radio galaxy 3C31. The contour interval is increased by a factor of 10 after the first 10 contours. Negative regions are shown hatched. *b*, Maximum-entropy map of 3C31, on the same scale as Fig. 1*a*. The contour interval is increased by a factor of 10 after every set of 10 contours, so that there are 750 of the lowest contours to the peak. The box shows the region covered by Fig. 1*c*. *c*, The central region of 3C31, analysed by the maximum entropy-algorithm. The contour levels are the same as in Fig. 1*b*.

sorted into piles, different maps being placed in different piles. Because we have quantised the space and intensity levels, there are only a finite number of such piles. We continue this process until each conceivable, compatible map has turned up many times, and then select the maps in the largest pile as the most likely representation of the sky.

The map most frequently produced by the monkeys has a uniform intensity. This procedure, therefore, produces the most uniform map consistent with the data. Indeed, if the noise in the data is larger than any real signal from the sky, then the uniform map will be consistent with the data and is thus the maximum-entropy solution. Conversely, if there is a feature on a maximum-entropy map, and the errors have been correctly estimated, then there must be evidence for it in the data. In this sense the method is safe. However, it does not follow that features on a maximum-entropy map must correspond to real features in the sky. We show later an example where the true noise level is much greater than the value used in the analysis, and features arise from the interpretation of this noise as real signals. Similarly, features can arise from an ambiguity in incomplete data over two or more possible interpretations. In such cases the method selects the smoothest map, which is not necessarily correct.

For simplicity we write the equations for data in one dimension, the extension to two or more dimensions being immediate. Let m_j denote the intensity at point j of a test map and let M_k be the Fourier transform of m_j. Suppose that we have measurements of M_k, denoted by E_k, only on a subset of k-values, which we call A. There is no restriction on the domain A, which can be any set of points in k-space.

There is some dispute about the correct definition of the entropy. We believe that the arguments of Frieden[5] are correct for our problem. He concludes that the most probable map is that which maximises $-\Sigma_j\, m_j \log m_j$. This formula expresses the configurational entropy of a map; this is not the same as the thermodynamic entropy of a beam of photons, nor is it the same as the information-theoretical entropy loss on passing a signal through a filter. An alternative expression, $\Sigma_j \log m_j$ (ref. 6), has been widely used in maximum-entropy spectral analysis and has also been applied in radioastronomy. We find the arguments leading to this expression less compelling than those of Frieden for the radioastronomical problem. We shall discuss the foundations of the method further elsewhere.

The unconstrained maximisation of $-\Sigma_j m_j \log m_j$ results in all the m_j being equal to e^{-1}, and maximising it subject to the constraint that the M_k are consistent with the data produces our solution. It is this approach which differs from that of some others[5,7]. We do not attempt to fit the data exactly, because this introduces structure into the map arising solely from noise in the data. Exact fitting also implies the existence of numerous separate constraints, resulting mathematically in an unwieldy proliferation of Lagrange multipliers and preventing calculation of the solution in all but the simplest cases.

We assume instead that the data E_k have gaussian errors, with individual standard deviations σ_k. The statistic $\Sigma_{k\varepsilon A}\, |M_k - E_k|^2/\sigma_k^2$ then possesses a χ^2 distribution. The sum is taken over the set of points A at which there are observations. A large value of χ^2 indicates that the map is a poor fit to the data, while a very small value arises when the map fits the data too closely and includes features due solely to experimental error. The expected value of χ^2 is equal to the number of data values, and we use Lagrange's method of undetermined multipliers to constrain χ^2 to equal this while we maximise the entropy. Maximising

$$Q(\lambda) = -\Sigma_j m_j \log m_j - \frac{\lambda}{2} \sum_{k\varepsilon A} |M_k - E_k|^2/\sigma_k^2$$

with respect to m_j gives

$$m_j = \exp\{-1 + \lambda \sum_{k\varepsilon A} (E_k - M_k)/\sigma_k^2 \exp(2\pi ijk/N)\} \qquad (1)$$

The multiplier λ must be positive; the apparently arbitrary

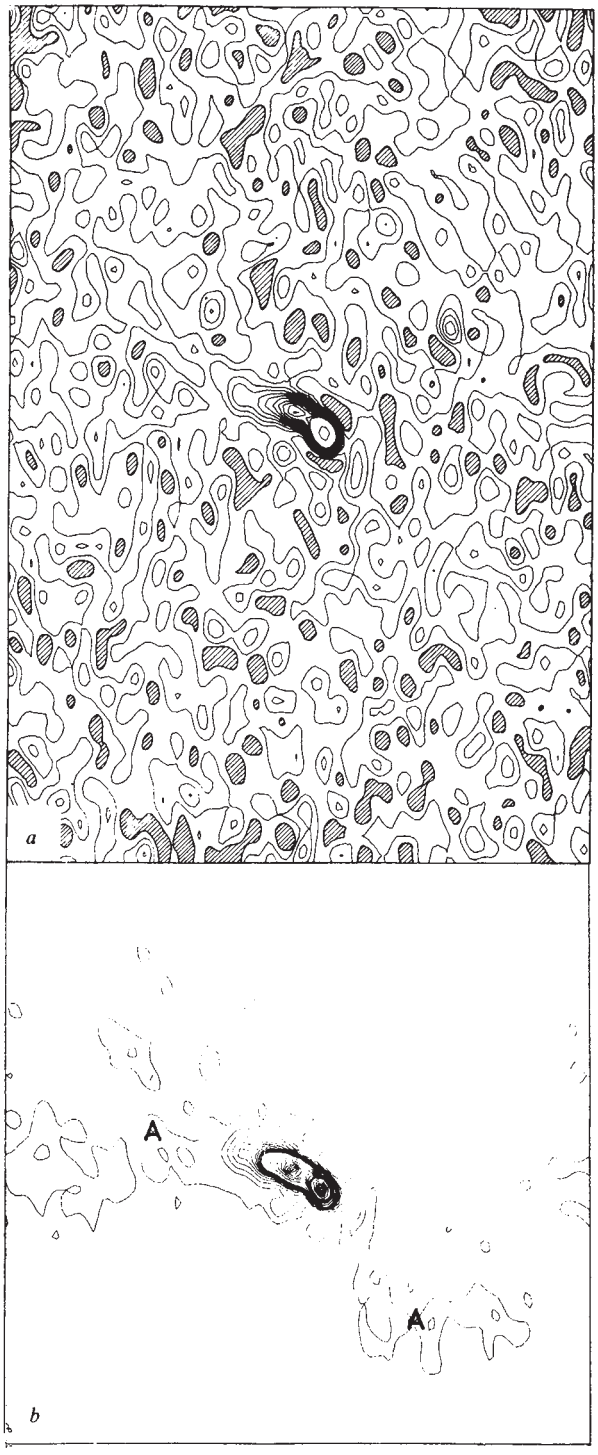

Fig. 2 *a*, Conventional map of 3C66. The contours are confused by fluctuations in the background, which are the result of receiver noise. Negative regions are shown hatched. *b*, Maximum-entropy map of 3C66. Regions of low surface brightness are now visible (A).

constant e^{-1} is related to the problem of the scaling of the data. This problem can be resolved by a more careful investigation of the foundations of the method.

Given E_k, σ_k and λ, this equation determines the intensities m_j on the map. It has been solved numerically by an iterative procedure, starting with the uniform map. Each new iterate is obtained by evaluating the right hand side of equation (1) with M_k equal to the Fourier transform of the previous iterate. We must average successive iterates to obtain convergence. The solution for a map of 128 × 128 grid points takes 3 min on the IBM 370/165 computer of the University Computer Laboratory, Cambridge. We can show that a solution of equation (1) must exist for any $\lambda > 0$, that it is unique and that it makes the quantity $Q(\lambda)$ a global maximum.

The correct value of λ makes χ^2 equal to the number of observations. During our iterative solution, λ is automatically increased until this is achieved by making it dependent on the current value of χ^2. In practice the solution is almost unchanged for a wide range of λ.

Applications using radioastronomical data

We have made extensive tests with simulated data. In every case the maximum-entropy reconstruction has been very similar to the original and we have found no cases where a misleading conclusion could have been drawn. We therefore present here some results using real observations made by the Cambridge radio telescopes. These data are incomplete because of the finite size of the telescope, because the data may be spoiled by electrical interference, or because the expense of further data collection outweighs the improvement to the final map of the sky. Errors in the data vary from sample to sample because of differing integration times and atmospheric conditions.

Figure 1*a* is a conventional map of the radio galaxy 3C31, observed at 1,407 MHz by the One-Mile Telescope[8]. The dynamic range is about 50:1. The shaded areas indicate negative regions, which arise principally as sidelobes of the main peak. Note the change in contour interval by a factor of 10 after the first 10 contours.

Figure 1*b* shows the maximum-entropy map produced with the same data. All negative sidelobes have been removed and positive ones greatly reduced, because these sidelobes arise from missing Fourier components and can be removed without affecting the fit to the data. The central peak is sharper and the noise background

Fig. 3 An example of the mis-use of the maximum-entropy method. The spurious features, which are not present in Fig. 2*b*, result from an over-optimistic estimate of the noise level in the data.

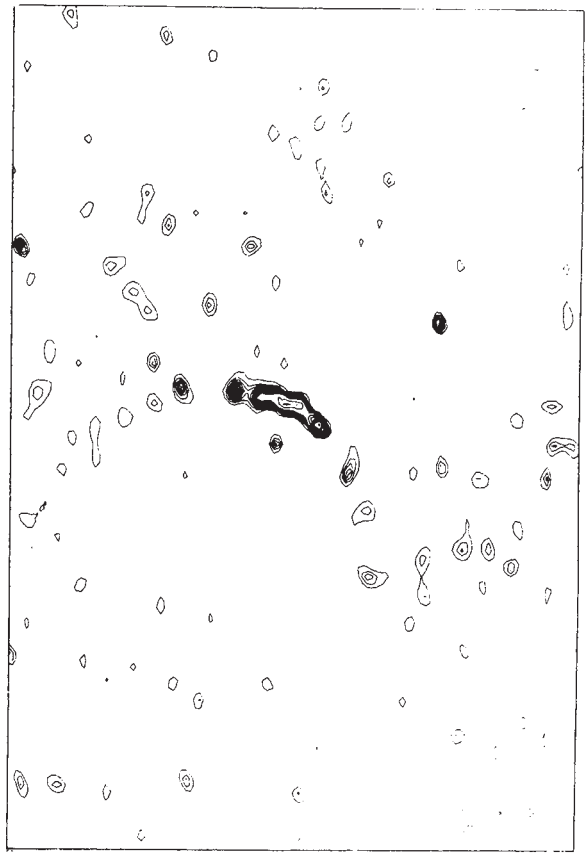

has been reduced, so that the apparent dynamic range is 1,000:1. An interesting feature is the valley A in Fig. 1*b*, which is barely visible in Fig. 1*a*. As our algorithm generates the flattest map consistent with the data we conclude that there is little evidence in the observations for a bridge connecting these two parts of the radio source. There may be one, but we need better data to see it.

A more detailed maximum-entropy map of the central part of this source is shown as Fig. 1*c*. To produce this we assume that our data come from the central part of a much larger radio telescope and that the Fourier components corresponding to the outer parts of the aperture are unknown. The algorithm now allows us to assign values to these unobserved Fourier components, but only in a way which makes the final map flatter. We see a further striking reduction in confusion caused by sidelobes, and a reduction in width of the main ridge of the source by a factor of about 2. This increase of resolution is attainable because, in Fig. 1*a*, the Fourier components corresponding to large spacings have been weighted down to one-third of their measured values to improve the sidelobe level, despite the consequent loss of resolution. In the case of 3C31, the extra details revealed by the algorithm are well confirmed by observations with higher resolving power[8]. A modest amount of 'super-resolution' is possible with this method if the signal-to-noise ratio is sufficiently high but any further increase in the size of the apparent aperture does not result in greater resolution. Because we consider noise in the data, we cannot get the implausibly high resolution that is suggested by some other methods of maximum-entropy spectral analysis[7].

Figure 2*a* shows the central region of the radio galaxy 3C66, observed at 5GHz by the One-Mile Telescope[9]. These data are much more noisy than those for 3C31 and the maximum-entropy map (Fig. 2*b*) shows only a very small increase in resolution. However, the map now shows clear evidence for more diffuse regions of lower surface brightness (marked A), as these are no longer confused by noise. The reality of these features is confirmed by observations at lower frequencies[9], where receiver noise is less of a problem.

Figure 3 shows a typical result if the experimental errors are seriously underestimated. To produce this unfortunate result, we assumed that each σ_k was five times smaller than that used to produce Fig. 2*b*. Noise in the data has now been interpreted as true signal and appears on the map. There is also some spurious 'super-resolution'. We include this picture to emphasise the dangers inherent in over-interpreting observational data. For the maximum-entropy method these dangers can be minimised by plotting a map of $|E_k - M_k|^2/\sigma_k^2$. Corrupted data then become obvious through their unacceptably large contributions to χ^2.

Maximum-entropy solutions without phase information

We have so far assumed that the observations E_k are complex numbers, and that their real and imaginary parts have equal and independent gaussian errors. This is unrealistic in many important radioastronomical applications. For example, at high frequencies the main source of uncertainty is the troposphere, which introduces unknown phase errors into the Fourier components without affecting their amplitudes. In extreme cases, such as in very long baseline radio interferometry or in X-ray crystallography, the phases are entirely unknown.

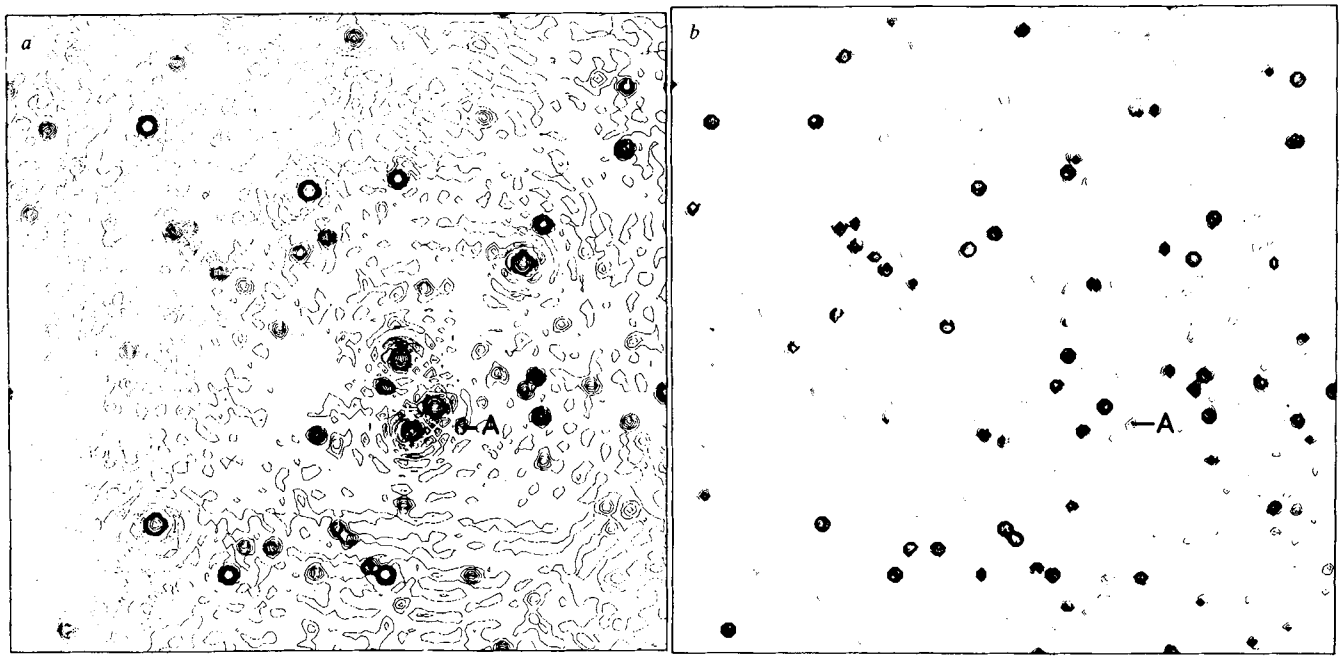

Fig. 4 *a*, Part of the 5C7 survey of radio sources. *b*, Phaseless maximum-entropy map of 5C7.

Under these circumstances, we use $\Sigma_{k\epsilon A}(|M_k| - A_k)^2/\sigma_k^2$ as a measure of the misfit to the data, where A_k denotes the observed amplitudes. Although this quantity does not have a χ^2 distribution, the number of observations is usually so large that we may apply the central limit theorem. The distribution is therefore approximately gaussian and its expectation value is easily estimated.

Maximising the entropy subject to the constraint that the misfit is equal to its expectation value yields

$$m_j = \exp\{-1 + \lambda \sum_{k\epsilon A} (A_k \exp(i \arg M_k) - M_k)/\sigma_k^2 \exp(2\pi ijk/N)\}$$

which may be solved by iteration in the same way as before. This time the solution is not unique; as well as the trivial cases of arbitrary translation or inversion of the solution, we have a technical counter-example (due to Dr J. Skilling) suggesting that the entropy may sometimes have more than one local maximum. We have, however, encountered no such ambiguity in our tests with realistic radioastronomical data.

Figure 4*a* shows part of the radio survey 5C7 (ref. 10), made with the One-Mile Telescope at 1,407 MHz. This map has been produced in the conventional manner, using the observed amplitudes and phases. The maximum-entropy map (Fig. 4*b*) has been

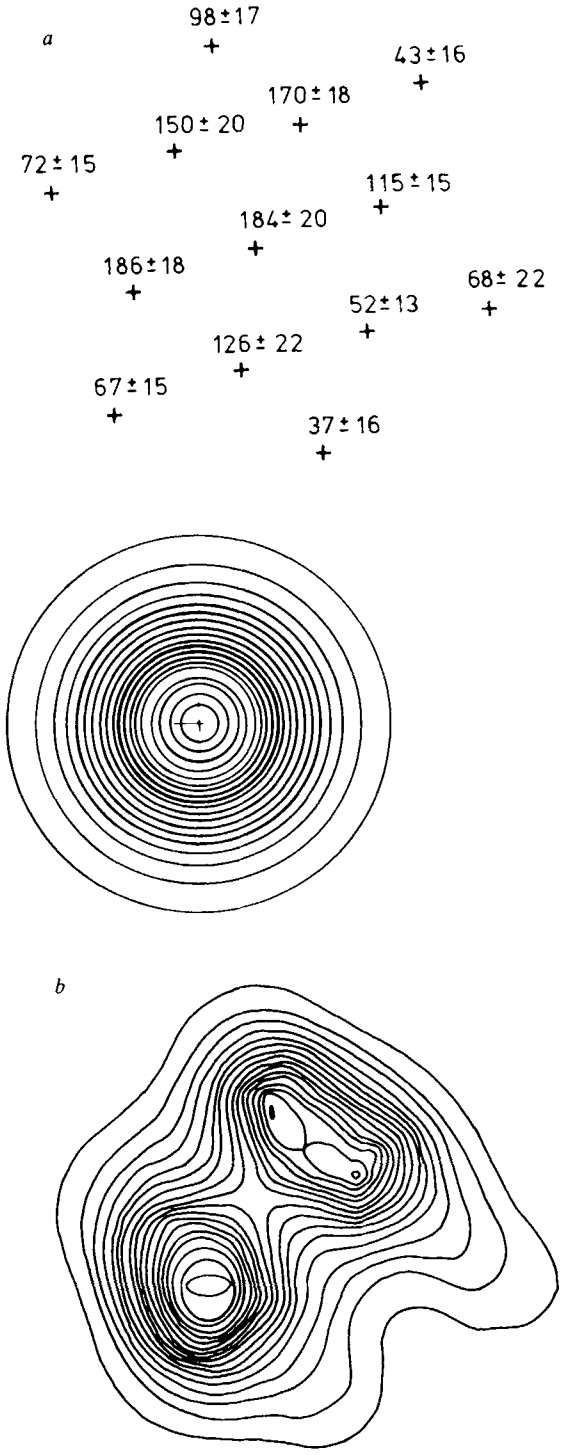

Fig. 5 *a*, X-ray counting rates for various positions near the supernova remnant Cassiopeia A. Also shown are the experimental errors, and a contour map of the point-spread function. *b*, Maximum-entropy X-ray map of Cassiopeia A on the same scale as Fig. 5*a*.

made utilising only the amplitude information. The phases were in fact given to the program, but only to start the iteration near the correct solution and to encourage it to produce its solution in the same orientation and position as Fig. 4*a*. Test cases show that the algorithm produces the correct solution even if no phase information whatever is given, although convergence is slower. All the sources visible on the conventional map have been reproduced, and most have the correct positions and flux densities. A few of the weak sources ($< 1\%$ of the brightest) have a slightly lower flux density on the maximum-entropy map; an example is marked A. Presumably, evidence for the presence of this weak source cannot be extracted from these very incomplete data in the absence of phase information. The same radio survey has also been analysed by Baldwin and Warner[11], using a method similar to those used in X-ray crystallography. Both reconstructions closely resemble the true map, but ours has the anticipated features of good resolution and large dynamic range.

Further applications

The combination of maximum-entropy analysis with a proper treatment of experimental errors thus promises to be a powerful, yet safe, method for estimating the Fourier transform of incomplete and noisy data. For radioastronomical data, the scheme offers considerable advantages over other reconstruction techniques, for example, the CLEAN algorithm[12]. Because our algorithm produces a well-defined map even if the phases are entirely unknown, it is also ideal for the reconstruction of images produced by very long baseline radio interferometry, X-ray crystallography and speckle-pattern interferometry. Full technical details of our algorithm for the case of Fourier data will be given elsewhere.

The method is very easily generalised to deal with other types of data, not involving a Fourier transform. A particularly important example is the case where the data collected ($E_k \pm \sigma_k$) are the convolution of the required map with a known point-spread function or beamshape. The extension of the maximum-entropy method to this case is quite straightforward and yields

$$m_j = \exp\{-1 + \lambda \sum_{k \in A} B_{k-j}(E_k - g_k)/\sigma_k^2\}$$

where $g_k = \Sigma_j m_j B_{k-j}$ and B_j is the point-spread function. The maps are again smooth and give resolution limited by the signal-to-noise ratio. In this sense the solutions are far superior to those produced by the commonly used 'algebraic reconstruction technique'[13]. The maximum entropy-solution is again unique.

Immediate applications of this deconvolution technique exist in many branches of physics. As an example, we show an X-ray map of the supernova remnant Cassiopeia A, observed by the Copernicus satellite[14] and previously reconstructed by the ART algorithm[15]. The map is based on only 13 data points, which are shown in Fig. 5*a*, together with the point-spread function. The maximum-entropy map is shown as Fig. 5*b*, and resolves the supernova remnant into two major regions of X-ray emission. This reconstruction in fact resembles that produced by the ART algorithm[15], but is virtually identical to the radio map of the supernova at the same resolution.

In this simple example only 64×64 grid points are needed to show the full details of the maximum-entropy solution. However, the computer time required implies that there is no difficulty in processing pictures of up to 256×256 grid points and therefore that that digital processing of photographs by this algorithm is realistic with a fast computer.

We thank the Radio Astronomy Group for helpful comments, also Dr J. Skilling for proof of the existence and uniqueness of maximum-entropy solutions.

Received 2 November 1977; accepted 12 January 1978.

1. Parker, R. L. *A. Rev. Earth Planet. Sci.* **5**, 35 (1977).
2. Oldenburg, D. W. *Geophys. J. R. astr. Soc.* **44**, 413 (1976).
3. Jaynes, E. T. *Phys. Rev.* **106**, 620 (1957).
4. Jaynes, E. T. *Phys. Rev.* **108**, 171 (1957).
5. Frieden, B. R. *J. opt. Soc. Am.* **62**, 511 (1972).
6. Abels, J. G. *Astr. Astrophys. Suppl.* **15**, 383 (1974).
7. Burg, J. P. thesis, Stanford Univ. (1975).
8. Burch, S. F. *Mon. Not. R. astr. Soc.* **181**, 599 (1977).
9. Northover, K. J. E. *Mon. Not. R. astr. Soc.* **165**, 369 (1973).
10. Pearson, T. J. & Kus, A. J. *Mon. Not. R. astr. Soc.* **182**, 273 (1978).
11. Baldwin, J. E. & Warner, P. J. *Mon. Not. R. astr. Soc.* **182**, 411 (1978).
12. Högbom, J. A. *Astr. Astrophys. Suppl.* **15**, 417 (1974).
13. Stevens, J. C. & Garmire, G. P. *Astrophys. J.* **180**, L19 (1973).
14. Fabian, A. C., Zarnecki, J. C. & Culhane, J. L. *Nature phys. Sci.* **242**, 18 (1973).
15. Charles, P. A., Culhane, J. L. & Fabian, A. C. *Mon. Not. R. astr. Soc.* **178**, 307 (1977).